THE JOURNAL OF PHYSICAL CHEMISTRY B

Article

pubs.acs.org/JPCB

Modification of Alkanethiolate Monolayers by O(^{3}P) Atomic Oxygen: Effect of Chain Length and Surface Temperature

Hanqiu Yuan, K. D. Gibson, Wenxin Li, and S. J. Sibener*

The James Franck Institute and Department of Chemistry, The University of Chicago, 929 East 57th Street, Chicago, Illinois 60637, United States

ABSTRACT: We have conducted a comprehensive study of ground-state O(^{3}P) atomic oxygen reactions with 1-hexadecanethiolate ($CH_3(CH_2)_{15}SH$) and 1-undecanethiolate ($CH_3(CH_2)_{10}SH$) self-assembled monolayers adsorbed onto Au/mica substrates, using X-ray photoelectron spectroscopy, infrared reflection absorption spectroscopy, ellipsometry, and contact angle measurements. In general, the reactions are not limited to the terminal methyl groups. Apparently, the incident O(^{3}P) (translational energy per atom of 0.11 kJ mol^{-1}) can penetrate below the surface of the monolayer. The ability of the atoms to penetrate, and thus the reaction rate of the backbone $-CH_2-$, is dependent upon both the temperature and the chain length, with the longer chain having a large difference between the rate at room temperature and 150 K. In particular, the long-chain SAM exhibits clearly reduced reactivity with respect to the incident beam of atomic oxygen when the film is cooled to 150 K as compared to room temperature. This is a notable finding and demonstrates the crucial importance that structural order and dynamical fluctuations, both of which depend on chain length and substrate temperature, have in determining the surface passivation and protection characteristics of SAM overlayers with respect to attack by energetic reagents.

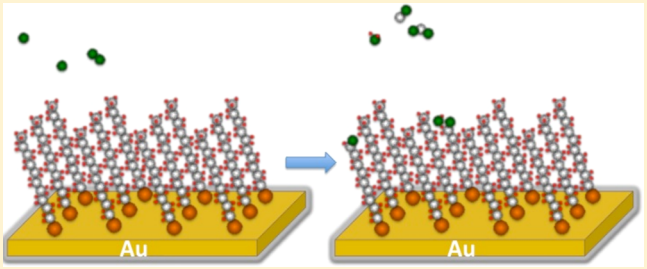

1. INTRODUCTION

Self-assembled monolayers (SAMs) are of great importance in a wide range of potential applications, from lithography[1] to biotechnological devices.[2] A thorough understanding of irradiation-induced modifications to SAM surfaces is relevant for further progress in these areas. Long-chain SAMs form highly ordered structures and can selectively expose different chemical functionalities at the surface. Because SAMs form ordered structures easily at the molecular scale, the control of the orientation and packing of the chemical functional groups on the surface can be used to tune the physical properties, such as adhesion, friction, and wettability.[3] These surfaces can also provide specific alignment toward heterogeneous reactions and gas−surface energy transfer and are thus of great importance to the study of gas−surface interactions.[4−7]

O(^{3}P) reactions with saturated hydrocarbons have been studied in both the gas and the condensed phases.[8−14] In this paper, we specifically discuss the reactions of O(^{3}P) atomic oxygen with alkanethiolate SAMs. A prior X-ray photoelectron spectroscopy (XPS) study of the interaction of O(^{3}P) (translational energy = 0.11 kJ mol^{-1}) with alkanethiolate SAMs[13] suggests considerable erosion of the film before there is any evidence of oxygen reaching the Au substrate. However, since their XPS system lacked the sensitivity to differentiate between the terminal methyl groups and the alkyl chain matrix, it is uncertain whether the reaction starts from the topmost layer, exposing a fresh etch front as the reaction propagates, or if some oxygen also penetrates into the SAM matrix before reaction is initiated. Penetration of O(^{3}P) into the SAM matrix has been demonstrated both theoretically[15,16] and experimentally.[13,17] For example, by selectively deuterating different carbons on a dodecyl SAM, it was found that, for O(^{3}P) with a translational energy of ∼0.16 kJ mol^{-1}, as much as ∼40% penetrated to the region between C_3 and C_6 (C_1 is the surface).[17]

In the present study, we elucidate how the reaction of low-energy O(^{3}P) with alkanethiolate SAMs on gold surfaces is initiated and propagates, and how factors such as surface temperature and chain length affect reactivity. To understand the microscopic nature of the O(^{3}P)-induced chemical events in the alkanethiolate SAMs, we used an infrared reflection−absorption spectrometer (IRRAS)[18] that permitted the in situ examination of the film composition and structure during the exposure. IRRAS has the advantage of distinguishing between reactive sites within the film and those at the film−vacuum interface, providing information otherwise unavailable through XPS; this capability was used to examine reactivity at various sites along the carbon backbone of the SAM. Moreover, the roles that structural disorder and dynamical fluctuations play in film reactivity, including the mechanistic basis for such effects, are critically examined. In situ XPS and ex situ ellipsometry measurements were also used to provide complementary information averaged over the entire SAM film.

Special Issue: B: Paul F. Barbara Memorial Issue

Received: July 15, 2012
Revised: September 18, 2012
Published: September 21, 2012

2. EXPERIMENTAL SETUP

2.1. SAM Preparation. Polycrystalline gold on mica substrates (Agilent Technologies Inc.) were cleaned by UV-ozone, rinsed repeatedly with ethanol and blown dry with nitrogen, and then immediately immersed in a 1 mM ethanol solution of the thiol precursor at room temperature for at least 48 h. The SAMs were made from 1-hexadecanethiol, $CH_3(CH_2)_{15}SH$ (C16), or 1-undecanethiol, $CH_3(CH_2)_{10}SH$ (C11) (Sigma-Aldrich, as received). After immersion, the samples were repeatedly rinsed with distilled ethanol and blown dry with nitrogen, and then transferred to the ultra-high-vacuum (UHV) surface analysis chamber for $O(^3P)$ exposure and surface analysis.

2.2. Oxygen Beam and Reaction. In situ experiments were conducted in a molecular beam scattering apparatus that consisted of a UHV chamber and a supersonic molecular beamline. A detailed description has been provided in a previous publication,[18] so only a brief description including the relevant modifications is included here.

A radio frequency plasma source[19] was used to generate a supersonic atomic oxygen beam formed by expanding 5% O_2 in Ne (60 Torr stagnation pressure) through a custom designed water-cooled quartz nozzle. The beam formed a 3 mm circular spot on the sample surface. The extent of oxygen dissociation was 44 ± 3% (determination of the dissociation percentage is described in detail in Sibener et al.[19]), with a flux of 2.5×10^{14} O atoms cm^{-2} s^{-1} and an average translation energy ($<E_{trans}>$) of 0.11 kJ mol^{-1} with the full width at half-maximum extending from 0.08 to 0.15 kJ mol^{-1}. The flux was determined from the pressure rise in the third differential pumping region of the beamline. Any residual ionic species were removed from the beam by using a deflector plate biased at 2.0 kV. For control experiments, a molecular oxygen beam with no plasma and a pure neon plasma beam were used; neither caused a change in the SAMs. Sample exposure was done at normal incidence.

2.3. Sample Analysis. The in situ IRRAS and XPS analysis of SAM reactions were conducted in an ultra-high-vacuum (UHV) chamber. The sample was mounted on a five-axis manipulator, which could be cooled below 120 K with liquid N_2, and heated radiatively to 600 K.

The IRRAS spectra were obtained using a Nicolet model 6700 infrared spectrometer with a liquid-nitrogen-cooled MCT/A detector using p-polarized light at a glancing incident angle of 75°. The atom beam intercepted the surface at the position of the IR so that spectra could be taken without interrupting the $O(^3P)$ exposure. IRRAS spectra were collected at a resolution of 4 cm^{-1} and averaged over 500 scans. The spectra characterizing the SAMs were taken in reference to bare Au substrates. The IRRAS spectra are all in reference to the unexposed SAM sample, and the resultant difference spectra show changes in IR absorption caused by the $O(^3P)$ reactions. Spectra were fit using a nonlinear least-squares fitting routine with Lorentzian line shapes.

XPS measurements were carried out in the same UHV chamber. X-ray irradiation is known to initiate electron-stimulated C−H, C−C, and S−Au bond breaking within SAMs and to compromise their structural integrity.[20] Therefore, XPS analysis was only carried out after $O(^3P)$ exposure and the spectra acquisition time was kept as short as possible so as to minimize the effects of the X-ray irradiation (SAM quality after XPS analysis was checked using IRRAS to ensure no significant modification). Spectra were acquired using an Al Kα (1486.6 eV) X-ray source (PHI model 04-151) operating at 10 kV and 200 W with an incident angle of 45° from the sample normal. XPS survey spectra were acquired using a double pass cylindrical mirror analyzer (PHI model 15-255G) with a pass energy of 100 eV and a step size of 10 eV. Spectra in the C 1s, S 2p, O 1s, and Au 4f regions were recorded with a pass energy of 50 eV and a step size of 0.1 eV. The energy scale was referenced to the intense Au $4f_{7/2}$ peak at 83.8 eV.[21] XPS data analysis was performed using a commercial software package employing Gaussian peak fitting and linear baseline subtraction.

By necessity, ellipsometry and contact angle measurements were made after the sample was removed from the vacuum. The average thickness of SAMs was measured at five different spots on each sample with a Gaertner L116S ellipsometer (λ = 633 nm, n_{SAM} = 1.5, $\tilde{n}_{Au}$ = 0.2246−3.5i). The wettability of the SAM surfaces was measured by static water contact angle measurements. Microliter droplets of DI water were applied at the sample surface by a syringe infusion pump (Harvard Apparatus), and measurements of the contact angle were made on both sides of the two-dimensional projection of the droplet, captured by a video camera with a microscope lens. Each reported angle is averaged over six measurements on the same substrate sample.

3. RESULTS

3.1. XPS Measurements of $O(^3P)$-Induced Modifications of SAMs. XPS characterization provides qualitative and semiquantitative analysis of the monolayer with sensitivity to elemental composition and the binding environment. Spectra of the C16 SAM before and after reactions are shown in Figure 1.

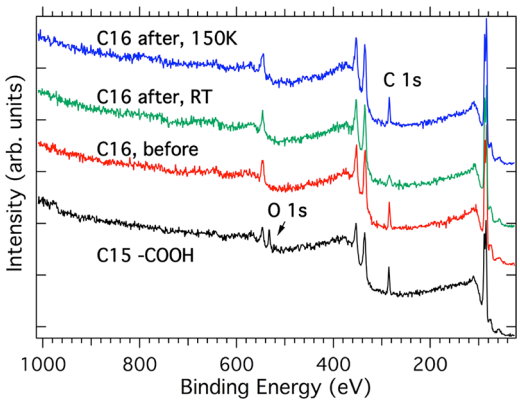

Figure 1. XPS survey spectra of the C16 SAM before and after $O(^3P)$ reaction (dose: 9.0×10^{17} atoms/cm^2) at RT and 150 K. As a comparison, a survey spectrum of a 16-mercaptohexadecanoic acid (C15-COOH) SAM is also displayed to show the O 1s oxygen peak.

Prior to $O(^3P)$ exposure, the primary feature of the survey spectrum is the presence of a single peak from the C 1s photoelectron centered at 284.6 eV. Au photoelectrons (4p, 4d, and 4f) from the substrate are also present, including a well-resolved Au $4f_{7/2, 5/2}$ doublet at 83.8 and 87.4 eV. The signal from the S 2p photoelectrons at 162 eV is not visible above the noise level. After $O(^3P)$ exposure, the C 1s peak decreased significantly and broadened at room temperature, while its intensity remained largely the same after exposure at 150 K. No peaks associated with oxygen were detected throughout the process. As a comparison, a survey spectrum of a 16-mercaptohexadecanoic acid (C15-COOH) SAM is shown in Figure 1.

dx.doi.org/10.1021/jp307005x | J. Phys. Chem. B 2013, 117, 4381−4389

Figure 2 shows the evolution of the C 1s peak as a function of O(^{3}P) exposure at different sample temperatures for both

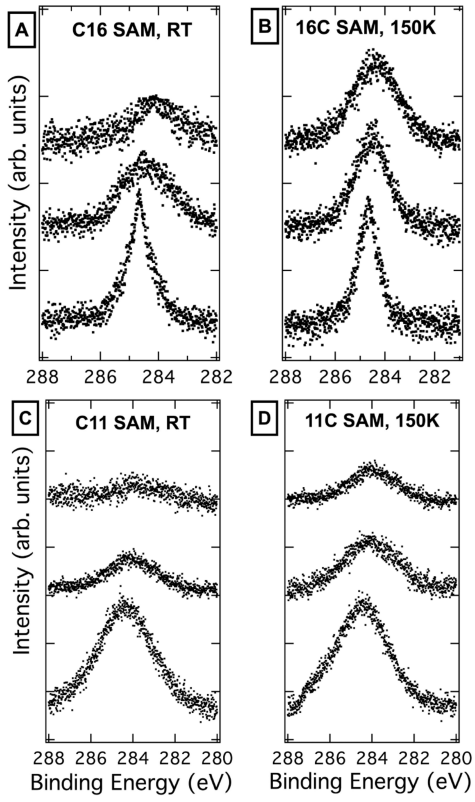

Figure 2. Evolution of the C 1s region of C16 and C11 SAMs as a function of O(^{3}P) exposure at RT and 150 K. In each panel from bottom to top, the O(^{3}P) doses are 0, 4.5 × 10^{17}, and 7.5 × 10^{17} (9.0 × 10^{17} in (A)) atoms/cm^2. The intensity axes all have the same scaling, and the spectra are offset for comparison (every 1 × 10^{17} atoms = 400 s).

C11 and C16 SAMs. Before exposure, the XPS spectrum of the C 1s feature of the C16 SAM shows a narrow, symmetric peak centered at 284.6 eV with a width of ~1.4 eV, in good agreement with literature values.[22] The C 1s peak of the pristine C11 SAM is slightly broader, which could be due to a slightly poorer surface ordering in a shorter-chain SAM or a stronger screening gradient close to the substrate.[23,24]

As O(^{3}P) exposure proceeds, the C 1s peak loses intensity, broadens, and shifts to a lower binding energy as the carbon backbone is reacted away. We feel that the decrease in peak intensity is due to the desorption of alkyl chain fragments rather than intact chains. This conclusion is supported by observations to be discussed later in this paper. The broadening of the peaks indicates an increasingly inhomogeneous chemical and structural environment. The peak shift toward lower binding energy when only a small fraction of the carbon remains indicates increasing dehydrogenation of the film.[20]

To quantify the changes, the effective length of the remaining C backbone during O(^{3}P) exposure could be approximated by the ratio of the C 1s to Au 4f integrated intensity, I(C 1s)/I(Au 4f, 5/2 and 7/2) (with an exponential attenuation of the photoelectron signal assumed).[25−28] For the SAMs with alkyl chains of carbon number n, the total C 1s XPS intensity, I_C, can be expressed as the sum of the signal, I_{CL}, from each of the individual methylene or methyl units in the monolayer attenuated by the overlying C atoms

$$I_C = \sum_{j=1}^{j=n} I_{CL} \exp\left(\frac{-(j-1)d_C}{\lambda_C}\right) \approx I_{C,bulk}\left[1 - \exp\left(\frac{-nd_C}{\lambda_C}\right)\right] \quad (1)$$

where d_C = 1.1 Å[28] is the thickness of one methylene or methyl layer, assumed to be the same in the present study, λ_C is the escape depth of C 1s photoelectrons through the carbon layer, and $I_{C,bulk}$ is the intensity of the C 1s peak from an infinitely thick carbon layer. The XPS Au signal is expressed as

$$I_{Au} = I_{Au,bulk} \exp\left(\frac{-(nd_C + d_S)}{\lambda_{Au}}\right) \quad (2)$$

where $I_{Au,bulk}$ is the unattenuated signal from a gold substrate and d_S is the thickness of the sulfur in the SAM. The electron escape depths of carbon and gold were determined from the empirical equation[28]

$$\lambda(\text{Å}) = 9.0 + 0.022\text{KE} \quad (3)$$

where KE stands for the kinetic energy of the photoelectrons of each element. This gives values of λ_C = 35.4 Å and λ_{Au} = 34.7 Å with Al Kα radiation. Values of I_{CL} and $I_{Au,bulk}$ were determined from XPS spectra with bare Au or SAM before reactions. The ratio of I_C and I_{Au} is used to determine n, the effective number of carbon atoms in each chain of the monolayer, if the tilt angle of the monolayer is assumed to remain at 33°. The results of this analysis, plotted as the effective number of C per chain remaining, is plotted in Figure 3.

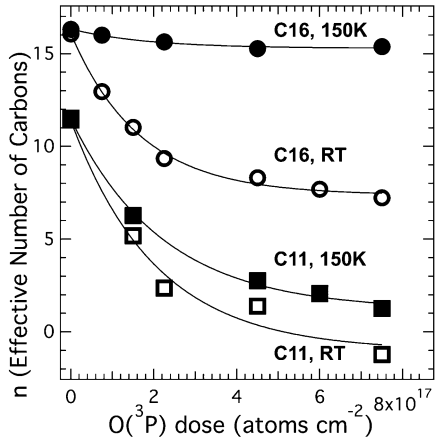

Figure 3. O(^{3}P) exposure dependence of the effective carbon number for C11 and C16 SAMs, determined as described in section 3.1. The lines are single-exponential fits (every 1 × 10^{17} atoms = 400 s).

The decrease in C per chain can be fit with first-order decay curves. At room temperature, nearly the same rate of decrease is observed for the two different chain lengths. This implies that the depletion of intact thiol chains is not the main reaction pathway in the present study since the thickness change would have been proportional to the original chain length of SAMs in that scenario. At 150 K, the rate for C11 SAMs has hardly changed, while the rate for the C16 SAMs has greatly decreased.

dx.doi.org/10.1021/jp307005x | J. Phys. Chem. B 2013, 117, 4381−4389

A strong temperature dependence of the reaction rate was seen in a previous study of $O(^3P)$ reactions with Langmuir–Blodgett (LB) films and SAMs.[14] One possibility for the well-ordered C16 SAMs is that, as the vibrational amplitude of the chains increases with increasing temperature, channels that can easily accommodate the O atoms open up, allowing for easier penetration into the SAMs. This leads to an increased reaction rate with the $-CH_2-$ of the alkanethiolate backbone. At the lower temperatures, O atoms cannot readily penetrate below the surface of the well-ordered C16. The C11 overlayer is less ordered, and O can still easily penetrate below the surface, even at the lower temperatures.

3.2. IRRAS Measurements of $O(^3P)$ Modifications of SAMs. The ability of our IRRAS setup to characterize the changes occurring in organic thin films has been previously demonstrated.[18] Spectral features, such as the peak intensity, position, and width of the C–H stretch modes of SAMs, are sensitive parameters of chemical and structural changes in the films.

Figure 4 shows the IRRAS spectra in the C–H stretching region for C16 and C11 SAMs on polycrystalline gold

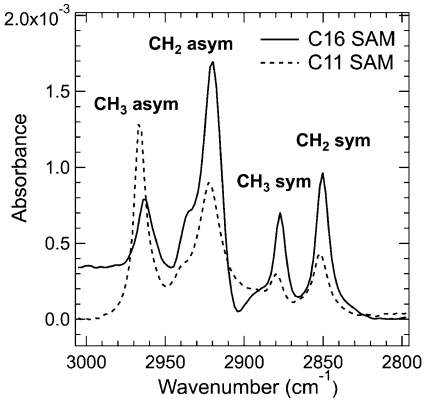

Figure 4. IRRAS spectra of C16 and C11 SAMs on polycrystalline Au substrates, as deposited.

substrates. Consistent with the IRRAS results for alkanethiolate SAMs, each spectrum is dominated by five absorption bands: CH_2 symmetric stretch ($\nu_s(CH_2)$, 2850 cm^{-1}), CH_3 symmetric stretch ($\nu_s(CH_3)$, 2876 cm^{-1}), CH_2 asymmetric stretch ($\nu_a(CH_2)$, 2919 cm^{-1}), Fermi-resonance coupled symmetric CH_3 stretch (2936 cm^{-1}), and in-phase and out-of-phase asymmetric CH_3 stretch ($\nu_a(CH_3)$, 2955–2965 cm^{-1}). These assignments and the polarizations of the individual bands are in excellent agreement with literature values of crystalline alkanethiolate-Au SAMs.[29,30]

There are two main differences between the two SAMs. First, $\nu_s(CH_2)$ and $\nu_a(CH_2)$ of the C16 SAM increase in intensity and red shift compared with the C11 SAM. This is directly related to the increase of methylene units, while the red shift is indicative of an increase of order in the monolayer due to increased van der Waals interactions among the chains as the chains increase in size.[30] The other difference is the relative intensities of $\nu_s(CH_3)$ and $\nu_a(CH_3)$ on the two SAMs. The greater $\nu_a(CH_3)$ intensity of the C11 SAM relative to that of the C16 SAM originates from the "odd–even" effects of SAMs, since $\nu_a(CH_3)$ has a transition dipole moment that is more normal to the surface in SAMs with an odd number of backbone carbons.[31]

The effects of $O(^3P)$ exposure on the IRRAS spectra of C16 and C11 SAMs are shown in Figure 5. $O(^3P)$ exposure of SAMs induced decreases to all the C–H stretch modes both at room temperature and at 150 K. The decreases of methyl and methylene C–H modes are concurrent, indicating that the reaction initiation is not limited to the terminal groups. The positive feature at the shoulders of some negative peaks are due to peak broadening, an indication of disordering of the monolayer.[32]

Before we use the IRRAS results to quantitatively study the rates of $O(^3P)$ reactions with SAMs, there are some issues to consider. First, surface temperature dependence of the C–H stretch modes has to be factored in. As discussed above, the peak position, integrated intensity, and width of the IRRAS spectral features are sensitive to the SAM's structural parameters. Low surface temperature has been shown to affect the structure of alkanethiolate SAMs on Au mainly through increasing tilt angle and decreasing gauche defects.[33] The integrated intensity ratio of each C–H stretch peak at 150 K to that at room temperature is determined. This ratio, $R_{RT/150\ K}$, is used to normalize all peak intensities to their room-temperature values. This value is different for C16 and C11 SAMs—the C16 SAM showed an ~30% increase in intensity at 150 K, whereas the C11 SAM modes only increased ~10%—and is slightly different for different modes on the same SAM.

Second, we need to consider whether the changes in the IR peaks are due to a decrease in density or due to changes in orientation. The intensity of absorption bands in IRRAS depends not only on the number of molecules (concentration) but also on the orientation of the molecules (surface selection rule). Any disruption or disordering of the chains will cause the chains to reorient, and hence the decrease in the C–H stretch modes could not be simply attributed to dehydrogenation or the loss of carbon moieties. Therefore, a combination of XPS and ex situ analysis, including ellipsometry and contact angle measurements, was used to complement the IRRAS data.

The reduced intensity of the C–H bands can be due to dehydrogenation, removal of the hydrocarbon components, and/or changes in the alkyl chain orientation. $\nu_a(CH_2)$ especially reflects the average CH_2 density and orientation throughout the entire film. $\nu_a(CH_3)$ has been shown to be linearly related to the number density of methyl terminal groups on the surface.[34] These two modes are usually used for quantitative interpretation. Compared with the effective thickness change from the XPS results, the IR plot of the $\nu_a(CH_2)$ peak area shows a very good correlation at the initial stages of reaction (Figure 6). Also shown is the intensity ratio of symmetric (in-plane to the CCC backbone plane) and asymmetric (perpendicular to the CCC backbone plane) C–H stretch of methylene units (I_{sym}/I_{asym})[29] for the room-temperature surface plotted as a function of $O(^3P)$ dose. In the initial stages of reaction, the relative intensity of the two modes remains essentially constant, indicating that the orientation of the alkyl chains relative to the substrate is not significantly altered and is not a major factor contributing to the decrease of the IR modes. After prolonged reaction, the apparent disparity between the XPS and the IR results is probably due to a change in angle between the remaining fragment of the carbon chain and the gold surface. The following discussion will focus, therefore, on the oxidation times where the XPS and IR experiments show the same apparent reaction rate, corresponding to the regime where the film structure is largely unchanged from its initial geometry.

dx.doi.org/10.1021/jp307005x | J. Phys. Chem. B 2013, 117, 4381–4389

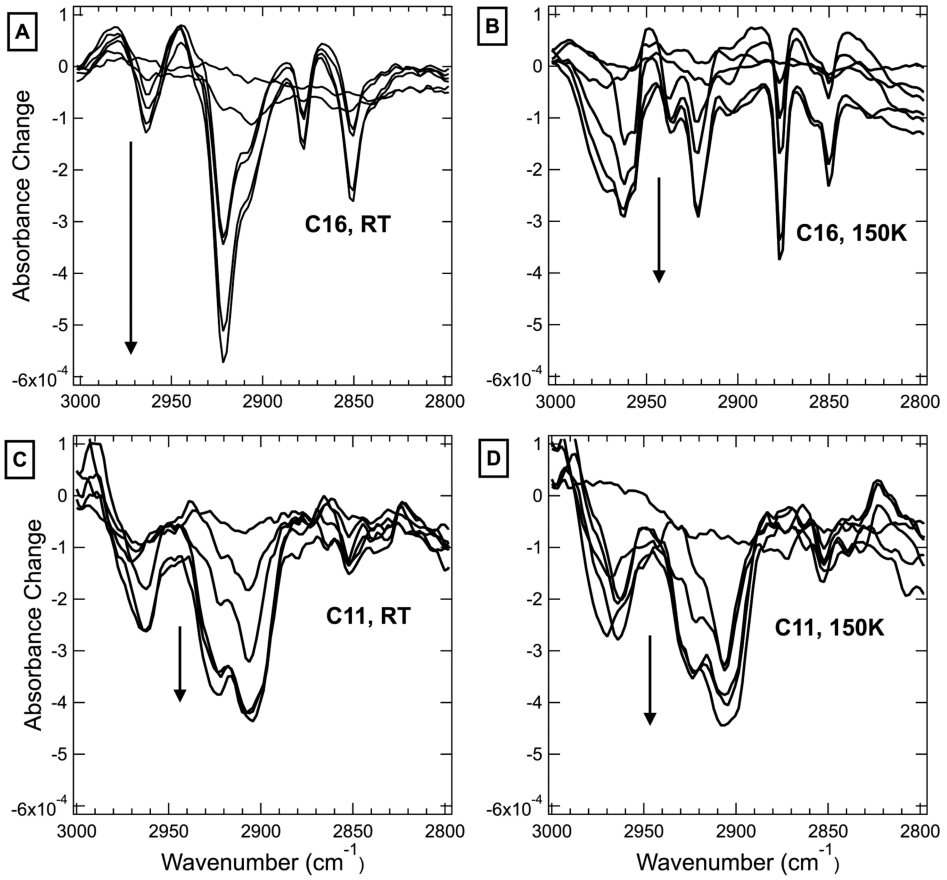

Figure 5. In situ IRRAS spectra of the C16 SAM ((A) at room temperature, (B) at 150 K)) and the C11 SAM ((C) at room temperature, (D) at 150 K) during $O(^3P)$ exposure. The same vertical scale is used for all figures. The difference spectra were obtained using the pristine SAMs as the reference. Negative peaks correspond to the loss of absorbing material from the film, positive peaks indicate new vibrational modes, and differential-shaped features indicate changes in peak position or width. There are no significant differences between the two spectra outside the 2800−3000 cm^{-1} region; this is true for all of the results presented in this work. From top to bottom, the $O(^3P)$ doses are 0, 0.3×10^{17}, 1.5×10^{17}, 3.0×10^{17}, 4.5×10^{17}, and 7.5×10^{17} atoms cm^{-2} (every 1×10^{17} atoms = 400 s).

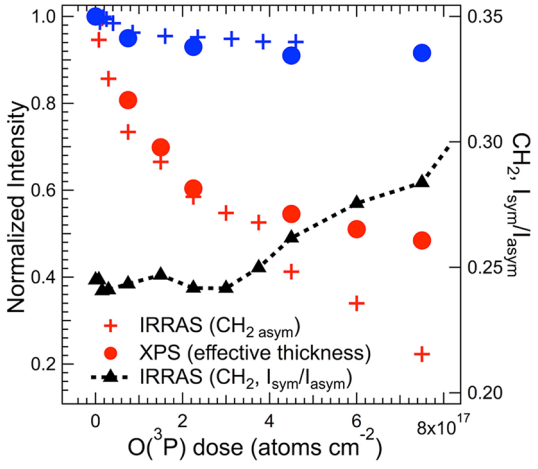

Figure 6. Correlation between the IRRAS integrated intensity of the asymmetric C−H stretch of methylene units and the effective thickness determined by XPS (filled circles) as a function of $O(^3P)$ exposure of the C16 SAM at room temperature (red) and at 150 K (blue). Both intensities are normalized to their respective values before reaction with $O(^3P)$. The ratio of the IRRAS intensity of asymmetric and symmetric C−H stretch modes of methylene units (crosses) is also plotted as a function of dose at room temperature. All the ratios are normalized to the values of a pristine SAM (every 1×10^{17} atoms = 400 s).

To quantify the reactivity from different functional groups, the rate of decrease of the C−H stretch peak area is plotted as a function of dose in Figure 7. It follows first-order reaction kinetics and could be expressed as

$$\Delta I = I_0(1 - e^{-k_{obs}t}) \quad (4)$$

where ΔI is the change in the integrated intensity (the integrated intensity in the "difference spectra") of the functional group at time t and I_0 is the original IR signal intensity and is a constant related to the SAM. The k_{obs} for the $\nu_s(CH_2)$ signal was found to be the same as that for the $\nu_a(CH_2)$ signal within 10%. The first-order kinetics agree with the XPS results.[14]

At room temperature, the rates are essentially the same for C16 and C11 SAMs. Also, the decreases of methyl and methylene IR peaks are concurrent. This indicates that the reaction is not limited to the vacuum−film interface with just the methyl terminal groups. This observation is consistent with previous studies that $-CH_3$ is not the most reactive site when $O(^3P)$ reacts with alkyl SAMs and that $O(^3P)$ initiates reactions by penetrating into the matrix and reacting with the alkyl chains.[15−17] At 150 K, the reaction rate for the C11 SAM is similar to that at room temperature. The terminal methyl groups did not show an increased reactivity, and $\nu_s(CH_3)$ did not show a disproportional decrease, indicating that the orientation of the terminal groups was not different from the reactions at room temperature.

dx.doi.org/10.1021/jp307005x | J. Phys. Chem. B 2013, 117, 4381−4389

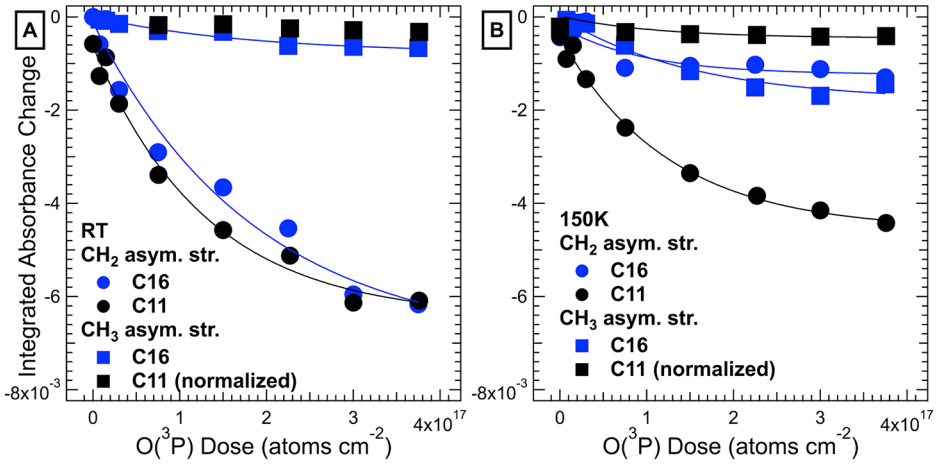

Figure 7. Decrease in the integrated intensity of the asymmetric stretch of methyl (square) and methylene (circle) during $O(^3P)$ exposure of the C16 SAM (blue) and the C11 SAM (black) at room temperature (left) and at 150 K (right). The spectra used for integration are all difference spectra and are referenced to the SAMs before reaction, as shown in Figure 5. The temperature effect on the C−H peak intensity is corrected so that the data points are normalized to the room-temperature values. The CH_3 intensity on the C11 SAM (red square) was corrected for the odd−even effect and was normalized to the values of the even-numbered SAM. The lines represent single-exponential fits and are representative of first-order kinetics (every 1×10^{17} atoms = 400 s).

In contrast, lowering the temperature of the C16 SAM resulted in a greatly reduced rate for the decrease in signal due to methylene, and a slightly increased rate of reaction of the methyl as compared with that at room temperature. The explanation for this is probably the same as that presented earlier in the section covering the XPS results; the better ordering of the longer SAM combined with the decreased thermal motions of the chain effectively blocked penetration of $O(^3P)$ below the surface. This can explain both the decreased methylene and the increased methyl reaction rates.

Gas−surface reactions are usually characterized by the reaction probability (R), which represents the ratio of collisions of $O(^3P)$ atoms with the surface that lead to reaction (C−H bond cleavage in this case) to the total number of collisions per second. For the SAMs, the number of "reactive" collisions is extracted from the rate constant. The total number of collisions per second per functional group was calculated from the flux of $O(^3P)$ and the area of collision, assuming a hard sphere model.[14] The reaction probability is

$$R = \frac{\#\text{ of "reactive" collisions}}{\#\text{ of total collisions}} = \frac{k_{obs}}{A_{collision}\Phi_{O(^3P)}} \quad (5)$$

where k_{obs} is the observed rate, $A_{collision}$ is the area of collision, and $\Phi_{O(^3P)}$ is the flux of $O(^3P)$ atoms.

The results for methylene and methyl groups on different SAMs and at different surface temperatures are listed in Table 1. Compared with literature values of the gas phase (methyl, 5.5×10^{-6}; methylene, 1.6×10^{-4}; 300 K),[35] we found that the reaction probability is higher for adsorbed SAMs than for gas-phase alkanes, especially for methyl groups, the reaction probability of which is about 3 orders of magnitude higher in SAMs. This is qualitatively similar to the results for Langmuir−Blodgett (LB) films[14] (methyl, 3×10^{-2}; methylene, 5×10^{-3}; 300 K). That the reaction probability is actually slightly higher for methyl groups than for the much more numerous methylene groups is a strong argument against the desorption of the whole alkyl chain being an important reaction channel under the conditions explored herein. This result is indicative of a collision complex in which the oxygen atoms are trapped in the alkyl chain matrix, allowing for a longer residence time, as compared to a gas-phase reaction, and other reaction mechanisms become possible.[36,37] The relative reactivity between methyl and methylene groups on the C16 SAM is highly dependent on the surface temperature, while the C11 SAM showed little surface temperature effect.

Table 1. Reaction Probability of $O(^3P)$ with C−H Functional Groups on SAMs

reactive site	reaction probability (R) (per $O(^3P)$ collision)
C16 SAM, $-CH_2-$, RT	4.1×10^{-3}
C16 SAM, $-CH_2-$, 150 K	5.6×10^{-4}
C16 SAM, CH_3, RT	5.1×10^{-3}
C16 SAM, $-CH_3$, 150 K	8.4×10^{-3}
C11 SAM, $-CH_2-$, RT	6.4×10^{-3}
C11 SAM, $-CH_2-$, 150 K	6.1×10^{-3}
C11 SAM, $-CH_3$, RT	7.6×10^{-3}
C11 SAM, $-CH_3$, 150 K	7.2×10^{-3}

3.3. Ex Situ Analysis of SAMs after $O(^3P)$ Exposure. Ex situ analysis of the film thickness and wettability provides further information on the reactions between $O(^3P)$ and SAMs (Table 2). Ellipsometry showed that, at room temperature, the absolute values of thickness decrease of the C16 and C11 SAMs were essentially the same after exposure. The same $O(^3P)$ dose

Table 2. Ellipsometry and Static Water Contact Angle Measurements of C16 SAM and C11 SAM before and after $O(^3P)$ Exposure at Room Temperature and 150 K[a]

SAM	thickness (Å)	water contact angle (θ_{water})
C16, before exposure	22.1 ± 0.6	107.2 ± 1.0°
C16, after exposure at RT	11.5 ± 1.3	71.6 ± 2.8°
C16, after exposure at 150 K	21.8 ± 0.5	100.1 ± 1.7°
C11, before exposure	13.2 ± 0.4	107.2 ± 1.0°
C11, after exposure at RT	0.8 ± 0.7	65.6 ± 0.5°
C11, after exposure at 150 K	2.4 ± 0.4	65.4 ± 1.3°

[a]The average thickness of the monolayers was measured at five different spots on each sample. Each water contact angle is averaged over six measurements on the same substrate sample.

dx.doi.org/10.1021/jp307005x | J. Phys. Chem. B 2013, 117, 4381−4389

resulted in the same thickness decrease on the C11 SAM at 150 K, but only about a 5% change in the C16 SAM thickness. The static water contact angle (θ_{water}) of a pristine C16 SAM is ~110°, consistent with the literature values of well-ordered, crystalline long-chain alkanethiolate SAMs adsorbed on Au.[29]

In the in situ analysis, neither XPS nor IRRAS showed the appearance of any peak associated with oxygen during O(^{3}P) exposure, indicating that oxygen addition is not a common process, or that oxidized functional groups are not stable. The θ_{water} of the modified C16 SAM at 150 K is only slightly lower, indicating that the surface is still hydrophobic.

The C16 SAM exposed at room temperature has a θ_{water} value of ~70°. Because XPS spectra did not show any oxygen peaks above the noise level, the respective amount was estimated to be no more than 7.5% of the oxygen in the topmost −COOH layer of the C15-COOH SAM (Figure 1). This oxygen concentration alone is not sufficient to reduce the static water contact angle to the measured value, since the measured θ_{water} of a binary SAM containing 10% of −COOH terminal groups (90% $-CH_3$ termination) was ~100°. The difference might be explained by the roughness and disordering of the reacted film.[38] An alternative interpretation is that, when exposed to the air, the carbon-centered radicals react with molecular oxygen to produce oxygen-containing groups at the monolayer surface. Similar phenomena have been observed on atomic hydrogen modified long-chain SAMs.[39]

The ellipsometry and contact angle results are the same for C11 SAMs modified at different surface temperatures, further confirming that the reaction processes are similar for the C11 SAM at different surface temperatures.

4. DISCUSSION

Reactions of O(^{3}P) with saturated hydrocarbons have been thoroughly investigated in the gas phase.[8,9,11] For low kinetic energy O(^{3}P), the principle reaction is hydrogen abstraction, leaving an OH and a C radical. The barriers for this reaction with primary and secondary hydrogens are 34 and 22 kJ mol^{-1}, respectively (the incident energy in our experiments is ~11 kJ mol^{-1}), whereas the C−C bond cleavage needs an activation energy higher than 150 kJ mol^{-1}. However, insertion reactions are certainly possible in, for example, cyclohexane clusters[37] and adsorbed alkylthiol SAMs.[13] The latter case is the most directly related to our results. Wagner et al.[13] found not only evidence of insertion but also that continued O(^{3}P) exposure led to carbon loss when using O(^{3}P) with an average kinetic energy of ~11 kJ mol^{-1}.

In this context, it is also important to note that there is both experimental[17] and theoretical[16] evidence for penetration of the O(^{3}P) well below the SAM surface. Waring et al.[17] exposed C12 SAMs to O(^{3}P) ($<E_{trans} \geq 16$ kJ mol^{-1}). Using C12 with various parts of the carbon chain deuterated and monitoring the OD production, they determined that as much as ~40% can penetrate into the region between C_3 and C_6. Tasić et al.[16] calculated that, for 47 kJ mol^{-1} O(^{3}P) at near normal angles of incidence (our samples were exposed at normal), ~50% of the atoms penetrated below a C10 SAM surface.

In the present study, IRRAS measurements show that decreases in the methylene and methyl C−H peaks are simultaneous, indicating reactions at both sites. Moreover, methyl and methylene groups show very similar reactivity at room temperature, indicating that the reaction is not limited to the vacuum−SAM interface. However, oxygen was not observed in either XPS or IRRAS, indicating that there is only a very low concentration, if any, of nonvolatile oxygen-containing species left after the reaction. Erosion of carbon is mainly due to the fragmentation of alkyl chains and the formation of volatile carbon-containing species, such as CO or CO_2.[40] Other possible reaction pathways for the alkyl radicals include carbon−carbon bonding reactions with other alkyl radicals and dehydrogenation.

The change of methylene/methyl ratios in the remaining monolayer films as a function of O(^{3}P) exposure is summarized in Figure 8. The methyl groups disappear faster than the methylene groups, which indicates that O(^{3}P) is not depleting the whole chain evenly, but principally reacting with the upper segment of the alkyl chain. The fastest decrease in the ratio is for the C16 SAM at 150 K, indicating that the reaction is localized near the terminal group. This is consistent with the observation that the net decrease of methylene groups is either the same (at room temperature, Figure 7a) or smaller (at 150 K, Figure 7b) in the C16 SAM than in the C11 SAM.

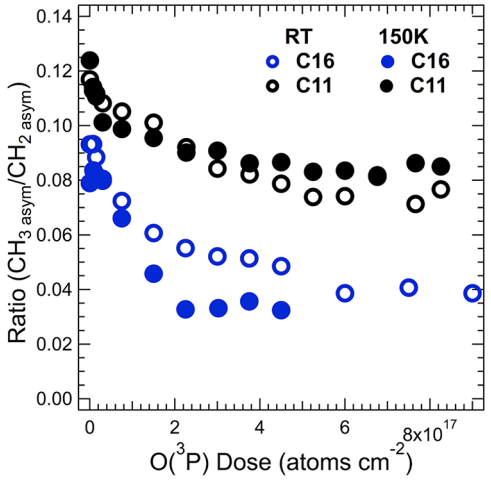

Figure 8. The ratio of the CH_2 asymmetric stretch and the CH_3 asymmetric stretch is plotted as a function of exposure on C16 and C11 SAMs at room temperature and 150 K. The ratios represent the relative intensity of methyl vs methylene groups that are left on the surface during reaction with O(^{3}P). The intensity changes due to temperature change and the odd−even effect were normalized to room temperature and even-numbered SAM values, as explained in section 3.2.

SAMs with different chain lengths respond to O(^{3}P) differently at different surface temperatures, indicating that chain length and surface temperature affect the reactivity. It has been shown that, in reactions between O(^{3}P) and organized organic thin films, the rate-determining step is the penetration of the oxygen between the chains;[14] thus, the structural difference induced by the chain length or surface temperature will affect the reactivity. The rate of oxygen transport through *n*-alkanethiolate SAMs on gold from cyclic voltammetry experiments has been shown to exhibit a strong chain-length dependence in their barrier properties.[41] The higher barrier properties of these films with increasing chain length have been attributed to the increased thickness of the films as well as to the increased crystallinity within the monolayers as observed by reflectance infrared spectroscopy.[29] Molecular dynamics (MD) simulations[42] showed that, for *n*-alkanethiolate SAMs for $n >$ 12, there is a middle region within these SAMs that adopted a more crystalline-like structure with a substantially lower gauche

dx.doi.org/10.1021/jp307005x | J. Phys. Chem. B 2013, 117, 4381−4389

defect density than in other parts of the monolayer. The thickness of this middle region was found to increase with chain length and yielded substantial enhancements in preventing oxygen diffusion. In contrast, shorter SAMs are much more disordered and less crystalline and thus allow a more rapid transport of oxygen.

Long-chain SAMs ($C \geq 16$) form a highly ordered structure as deposited. The gauche defects are near the top segments of the alkyl chains, allowing oxygen diffusion. At low surface temperatures, not only is oxygen diffusion slower but also the C16 SAM shows increased ordering, as compared with that at room temperature. This is evidenced by the increase in the C−H stretch mode intensity, indicating a higher titling angle and stronger van der Waals interactions between the alkyl chains.[33,43] On the other hand, shorter SAMs (C12 and below) are more disordered as deposited, only subject to reordering upon annealing.[43] Because of this, the relative reactivity of methyl and methylene groups remained the same for C11 SAMs at a lower surface temperature. The independence of methyl terminal group reactivity toward $O(^3P)$ with regard to surface temperature has been observed in organized organic thin films, though the limited studies have focused mainly on high temperatures.[14,36] At elevated temperatures, either the chains have greater mobility or the monolayer goes through a disordering phase transition, resulting in a increased penetration of $O(^3P)$ and higher reactivity. The effects of low surface temperatures have never been addressed.

Besides reaction with the hydrocarbon functional groups, it is important to consider whether oxygen diffuses to the SAM−Au interface and initiates reaction by oxidizing the sulfur−Au bond and causing desorption of intact alkyl chains. This reaction pathway has been shown to be the main process in the reaction of semifluorinated SAMs with low-energy $O(^3P)$,[13] but it is probably not a significant process in the present study. Neither Tasić et al.[16] (C10) nor Waring et al.[17] (C12) saw appreciable $O(^3P)$ penetration near the surface-bound S with $O(^3P)$ kinetic energies similar to what was used in our study. The IRRAS characterization clearly shows that the relative intensities of the methyl and methylene C−H stretch modes are different before reaction, mainly due to the longer chains of the C16 SAM (Figure 4). However, at room temperature, the absolute values of the methyl and methylene decreases in IRRAS are essentially the same on both SAMs regardless of chain length (Figure 7a). This clearly indicates that the removal of the entire alkyl chain is not a significant reaction pathway here, because the ratio of methyl and methylene decrease would have to be proportional to the original chain length, instead of being the same. Both XPS (Figure 3) and ellipsometry results (Table 2) also indicate that the main carbon desorption process is not via the depletion of intact alkyl chains. Similar trends have also been observed on low-energy electron-irradiated SAMs with different chain lengths,[20] indicating that the reaction is initiated from the upper segments of the alkyl chains. Reactions initiated at the SAM−substrate interface have a prolonged initiation period and would have probably resulted in different reaction rates on SAMs having different chain lengths.[13,39]

5. CONCLUSIONS

We studied the effect that ground-state atomic oxygen exposure (average kinetic energy of 0.11 kJ mol^{-1}) has on short-chain (C11) and long-chain (C16) SAMs at different surface temperatures. Complementary experimental techniques, including XPS, IRRAS, ellipsometry, and contact angle measurements, were used. Both methyl and methylene carbons react simultaneously, indicating that some of the $O(^3P)$ can penetrate between the chains. The cross sections for the irradiation-induced reactions were determined at the initial stage, and the loss of carbon exhibits first-order kinetics. There was no evidence that, at least initially for the pristine SAM, the oxygen could penetrate to the surface and react with the S, leading to desorption of the entire chain. For room-temperature exposure, C11 and C16 SAMs showed similar reactivity. In contrast, at 150 K, the reactivity of the C16 decreased much more than that of the C11. For the C16, reaction was particularly reduced for the methylene carbons, indicating decreased penetration of the $O(^3P)$. This demonstrates the crucial importance that structural order and dynamical fluctuations, both of which depend on chain length and substrate temperature, have in determining the surface passivation and protection characteristics of SAM overlayers with respect to attack by energetic reagents.

AUTHOR INFORMATION

Corresponding Author

*E-mail: s-sibener@uchicago.edu.

Notes

The authors declare no competing financial interest.

ACKNOWLEDGMENTS

This work was supported by the National Science Foundation, Award No. CHE-0911424. It is also a pleasure to acknowledge infrastructure support from the Materials Research Science and Engineering Center at The University of Chicago, NSF-DMR-0213745.

REFERENCES

(1) Kramer, S.; Fuierer, R. R.; Gorman, C. B. *Chem. Rev. (Washington, DC, U.S.)* **2003**, *103*, 4367−4418.
(2) Anker, J. N.; Hall, W. P.; Lyandres, O.; Shah, N. C.; Zhao, J.; Van Duyne, R. P. *Nat. Mater.* **2008**, *7*, 442−453.
(3) Gleiche, M.; Chi, L. F.; Fuchs, H. *Nature* **2000**, *403*, 173−175.
(4) Yan, T. Y.; Isa, N.; Gibson, K. D.; Sibener, S. J.; Hase, W. L. *J. Phys. Chem. A* **2003**, *107*, 10600−10607.
(5) Isa, N.; Gibson, K. D.; Yan, T.; Hase, W.; Sibener, S. J. *J. Chem. Phys.* **2004**, *120*, 2417−2433.
(6) Gibson, K. D.; Isa, N.; Sibener, S. J. *J. Chem. Phys.* **2003**, *119*, 13083−13095.
(7) Bosio, S. B. M.; Hase, W. L. *J. Chem. Phys.* **1997**, *107*, 9677−9686.
(8) Andresen, P.; Luntz, A. C. *J. Chem. Phys.* **1980**, *72*, 5842−5850.
(9) Luntz, A. C. *J. Chem. Phys.* **1980**, *73*, 1143−1152.
(10) Luntz, A. C.; Andresen, P. *J. Chem. Phys.* **1980**, *72*, 5851−5856.
(11) Ausfelder, F.; McKendrick, K. G. *Prog. React. Kinet. Mech.* **2000**, *25*, 299−370.
(12) Zhang, J. M.; Garton, D. J.; Minton, T. K. *J. Chem. Phys.* **2002**, *117*, 6239−6251.
(13) Wagner, A. J.; Wolfe, G. M.; Fairbrother, D. H. *J. Chem. Phys.* **2004**, *120*, 3799−3810.
(14) Paz, Y.; Trakhtenberg, S.; Naaman, R. *J. Phys. Chem.* **1994**, *98*, 13517−13523.
(15) Troya, D.; Schatz, G. C. *J. Chem. Phys.* **2004**, *120*, 7696−7707.
(16) Tasić, U. S.; Yan, T. Y.; Hase, W. L. *J. Phys. Chem. B* **2006**, *110*, 11863−11877.
(17) Waring, C.; Bagot, P. A. J.; Bebbington, M. W. P.; Raisanen, M. T.; Buck, M.; Costen, M. L.; McKendrick, K. G. *J. Phys. Chem. Lett.* **2010**, *1*, 1917−1921.
(18) Yuan, H. Q.; Killelea, D. R.; Tepavcevic, S.; Kelber, S. I.; Sibener, S. J. *J. Phys. Chem. A* **2011**, *115*, 3736−3745.

(19) Sibener, S. J.; Buss, R. J.; Ng, C. Y.; Lee, Y. T. *Rev. Sci. Instrum.* **1980**, *51*, 167−182.
(20) Zharnikov, M.; Grunze, M. *J. Vac. Sci. Technol., B* **2002**, *20*, 1793−1807.
(21) Wagner, C. D.; Riggs, W. M.; Davis, L. E.; Moulder, J. F.; Muilenberg, G. E. *Handbook of X-ray Photoelectron Spectroscopy*; Perkin-Elmer Corporation: Eden Prairie, MN, 1979.
(22) Bain, C. D.; Troughton, E. B.; Tao, Y. T.; Evall, J.; Whitesides, G. M.; Nuzzo, R. G. *J. Am. Chem. Soc.* **1989**, *111*, 321−335.
(23) Chesneau, F.; Zhao, J. L.; Shen, C.; Buck, M.; Zharnikov, M. *J. Phys. Chem. C* **2010**, *114*, 7112−7119.
(24) Heister, K.; Johansson, L. S. O.; Grunze, M.; Zharnikov, M. *Surf. Sci.* **2003**, *529*, 36−46.
(25) Dannenberger, O.; Weiss, K.; Himmel, H. J.; Jager, B.; Buck, M.; Woll, C. *Thin Solid Films* **1997**, *307*, 183−191.
(26) Hutt, D. A.; Leggett, G. J. *J. Phys. Chem.* **1996**, *100*, 6657−6662.
(27) Bain, C. D.; Whitesides, G. M. *J. Phys. Chem.* **1989**, *93*, 1670−1673.
(28) Laibinis, P. E.; Bain, C. D.; Whitesides, G. M. *J. Phys. Chem.* **1991**, *95*, 7017−7021.
(29) Laibinis, P. E.; Whitesides, G. M.; Allara, D. L.; Tao, Y. T.; Parikh, A. N.; Nuzzo, R. G. *J. Am. Chem. Soc.* **1991**, *113*, 7152−7167.
(30) Porter, M. D.; Bright, T. B.; Allara, D. L.; Chidsey, C. E. D. *J. Am. Chem. Soc.* **1987**, *109*, 3559−3568.
(31) Nuzzo, R. G.; Dubois, L. H.; Allara, D. L. *J. Am. Chem. Soc.* **1990**, *112*, 558−569.
(32) Peanasky, J. S.; McCarley, R. L. *Langmuir* **1998**, *14*, 113−123.
(33) Bensebaa, F.; Ellis, T. H.; Badia, A.; Lennox, R. B. *J. Vac. Sci. Technol., A* **1995**, *13*, 1331−1336.
(34) Truong, K. D.; Rowntree, P. A. *J. Phys. Chem.* **1996**, *100*, 19917−19926.
(35) Hampson, R. F. *Chemical Kinetic and Photochemical Data Sheets for Atmospheric Reactions*; U.S. Department of Transportation: Washington, DC, 1980.
(36) Paz, Y.; Trakhtenberg, S.; Naaman, R. *J. Phys. Chem.* **1992**, *96*, 10964−10967.
(37) Rudich, Y.; Hurwitz, Y.; Lifson, S.; Naaman, R. *J. Chem. Phys.* **1993**, *98*, 2936−2940.
(38) Ulman, A.; Evans, S. D.; Shnidman, Y.; Sharma, R.; Eilers, J. E.; Chang, J. C. *J. Am. Chem. Soc.* **1991**, *113*, 1499−1506.
(39) Gorham, J.; Smith, B.; Fairbrother, D. H. *J. Phys. Chem. C* **2007**, *111*, 374−382.
(40) Minton, T. K.; Zhang, J. M.; Garton, D. J.; Seale, J. W. *High Perform. Polym.* **2000**, *12*, 27−42.
(41) Zamborini, F. P.; Crooks, R. M. *Langmuir* **1998**, *14*, 3279−3286.
(42) Srivastava, P.; Chapman, W. G.; Laibinis, P. E. *Langmuir* **2009**, *25*, 2689−2695.
(43) Bensebaa, F.; Ellis, T. H.; Badia, A.; Lennox, R. B. *Langmuir* **1998**, *14*, 2361−2367.